

Unified deep learning network for enhanced accuracy in predicting thermal conductivity of bilayer graphene, hexagonal boron nitride, and their heterostructures

Cite as: J. Appl. Phys. **135**, 145106 (2024); doi: [10.1063/5.0201698](https://doi.org/10.1063/5.0201698)

Submitted: 31 January 2024 · Accepted: 22 March 2024 ·

Published Online: 12 April 2024



Rongkun Chen,¹ Yu Tian,¹ Jiayi Cao,¹ Weina Ren,^{1,a)} Shiqian Hu,^{2,a)} and Chunhua Zeng^{1,a)}

AFFILIATIONS

¹Faculty of Science, Kunming University of Science and Technology, Kunming 650500, People's Republic of China

²School of Physics and Astronomy, Yunnan University, Kunming 650091, People's Republic of China

Note: This paper is part of the special topic, Machine Learning for Thermal Transport.

a)Authors to whom correspondence should be addressed: wnren@kust.edu.cn; shiqian@ynu.edu.cn; and chzeng83@kust.edu.cn

ABSTRACT

In this research, we utilized density functional theory (DFT) computations to perform *ab initio* molecular dynamics simulations and static calculations on graphene, hexagonal boron nitride, and their heterostructures, subjecting them to strains, perturbations, twist angles, and defects. The gathered energy, force, and virial information informed the creation of a training set comprising 1253 structures. Employing the Neural Evolutionary Potential framework integrated into Graphics Processing Units Molecular Dynamics, we fitted a machine learning potential (MLP) that closely mirrored the DFT potential energy surface. Rigorous validation of lattice constants and phonon dispersion relations confirmed the precision and dependability of the MLP, establishing a solid foundation for subsequent thermal transport investigations. A further analysis of the impact of twist angles uncovered a significant reduction in thermal conductivity, particularly notable in heterostructures with a decline exceeding 35%. The reduction in thermal conductivity primarily stems from the twist angle-induced softening of phonon modes and the accompanying increase in phonon scattering rates, which intensifies anharmonic interactions among phonons. Our study underscores the efficacy of the MLP in delineating the thermal transport attributes of two-dimensional materials and their heterostructures, while also elucidating the micro-mechanisms behind the influence of the twist angle on thermal conductivity, offering fresh perspectives for the design of advanced thermal management materials.

© 2024 Author(s). All article content, except where otherwise noted, is licensed under a Creative Commons Attribution (CC BY) license (<https://creativecommons.org/licenses/by/4.0/>). <https://doi.org/10.1063/5.0201698>

INTRODUCTION

The thermal transport properties of layered materials have garnered considerable interest due to their pronounced anisotropy, which stems from the robust covalent bonds within the layers and the comparatively weak van der Waals interactions between them^{1–5}. This distinctive structure bestows upon these materials exceptional in-plane thermal conductivity coupled with a relatively diminished interlayer thermal conductivity, rendering them highly suitable for applications in electronic device heat dissipation. Graphene and hexagonal boron nitride (h-BN) are prominent among such materials, which excel in efficient in-plane thermal

management and safeguard the underlying circuitry against the perils of overheating^{6–10}. The ease with which these materials can be exfoliated and subsequently stacked in rotational arrangements further gives rise to moiré superlattices, possessing captivating electronic and thermal attributes^{5,11–22}.

The advent of moiré superlattices has precipitated an intensive wave of research focused on unraveling their unique electronic and thermal behaviors. Notable findings include the observation of Van Hove singularities in twisted graphene configurations, as well as the intriguing superconductor-to-insulator transition brought about by interlayer resonance enhancement.²³ Furthermore, the substantial reduction observed in thermal conductivity, alongside the marked

15 February 2025 11:32:22

enhancement in thermoelectric performance within moiré superlattices, has been associated with novel umklapp scattering processes tied to alterations in the Brillouin zone^{19,24–26}. Concurrently, van der Waals (vdW) heterostructures have emerged as a focal point of investigation, often exhibiting performances that either surpass or fall short of those exhibited by their constituent parent materials.^{27–32} The capacity to modulate physical properties through straightforward stacking techniques is particularly alluring, and studies have revealed that the creation of vdW heterostructures significantly alters interlayer interactions, thereby profoundly influencing the thermal transport characteristics of the system. Examples include the temperature-dependent decrease in thermal resistance at the interface between graphene and two-dimensional SiC,³³ as well as the complex issue of thermal current convergence within graphene and h-BN heterostructures.^{34,35}

Additionally, thermal transport studies typically rely on precise computational frameworks such as the Density Functional Theory (DFT)³⁶ and empirical potential-driven Molecular Dynamics (MD) simulations.³⁷ However, despite the high precision of DFT, its computational demands restrict the scale of systems that can be explored. On the other hand, while MD simulations accommodate larger systems, they often lack the comprehensive accuracy and applicability of DFT.^{38,39} Moreover, investigations into moiré superlattice systems necessitate precise descriptions of the variations in interlayer coupling caused by twisting,^{33,40–44} as well as addressing the increased atom count within the primitive cell and the concomitant escalation in computational costs due to reduced symmetry.^{45,46} It is evident that a method capable of delivering DFT-level precision, while achieving the computational efficiency of MD simulations is required. Relying solely on DFT would result in prohibitively high computational expenses, whereas exclusive dependence on MD might not guarantee the necessary level of accuracy. Particularly when describing interlayer coupling, the conventional Lennard-Jones (L-J) potentials may prove inadequate to ensure veracity.^{47,48} Thus, there is an urgent need for a novel approach that strikes a balance between computational precision and cost.

Recent advances in machine learning represent a promising solution, capable of achieving the accuracy of DFT, while retaining the computational efficiency of MD. Notable methodologies such as the Behler–Parrinello neural network (BPNN),⁴⁹ Gaussian Approximation Potential (GAP),⁵⁰ Gradient Domain Machine Learning Potential (GDMLP),⁵¹ Matrix Tensor Potential (MTP),⁵² Deep Learning Molecular Dynamics (DeepMD),⁵³ and Neural Evolutionary Potential (NEP)⁵⁴ represent key frameworks in this domain. For instance, the universal C element machine learning model, developed within the Gaussian Approximation Potential (GAP) framework,⁵⁵ along with the MLP crafted under the Neural Evolutionary Potential (NEP) framework specifically for layered h-BN,⁵ have both achieved near-DFT level accuracy, while substantially curtailing computational expenditures. Although MLP has been successfully applied to layered systems such as graphene and h-BN, its application within twisted graphene and h-BN heterostructures remains somewhat limited. This limitation stems from the intricate potential energy landscapes of heterostructures' twisted systems and the feeble long-range van der Waals forces, which collectively pose significant challenges in devising appropriate machine learning potential functions.^{56,57}

In this research, we employed DFT to conduct rigorous *ab initio* molecular dynamics (AIMD) simulations and detailed static calculations on graphene, h-BN, and their complex heterostructures. These materials were carefully subjected to a range of mechanical strains, perturbations, twist angles, and defects to gain a comprehensive understanding of their behavior. Utilizing the wealth of energy, force, and virial data obtained from these simulations, we constructed a meticulously curated training set encompassing 1253 distinct structural configurations. By harnessing the power of the NEP framework, seamlessly integrated within the Graphics Processing Units Molecular Dynamics (GPUMD) environment, we developed a highly accurate machine learning potential (MLP) model. This model faithfully mirrored the intricate potential energy surface predicted by DFT, ensuring both precision and reliability in our subsequent analyses. Thorough validation procedures, including the meticulous examination of lattice constants and phonon dispersion relations, further confirmed the robustness of our MLP model. This solid foundation enabled us to further explore the intricate thermal transport properties of these two-dimensional materials and their heterostructures. Our in-depth analysis revealed a profound impact of twist angles on thermal conductivity, particularly evident in heterostructures where a reduction exceeding 35% was observed. This substantial decline can be attributed to the twist angle-induced softening of phonon modes, coupled with a concurrent surge in phonon scattering rates. These phenomena collectively intensify the anharmonic interactions among phonons, significantly altering their transport properties. Our research not only underscores the remarkable efficacy of MLP models in elucidating the intricate thermal transport behavior of two-dimensional materials and their heterostructures but also provides valuable insights into the fundamental micro-mechanisms governing the influence of twist angles on thermal conductivity. In contrast to previous studies such as the universal Si MLP developed by Li *et al.*,⁵⁸ our research methodology is meticulously tailored to accommodate the unique properties of CBN elements and subsequent structures like twisted graphene and hexagonal boron nitride heterostructures. By adopting the Neural Evolution Potential (NEP) framework for constructing a unified descriptor, our approach aims to capture the complex interactions present in these systems, thereby broadening the scope of problems that our MLP can effectively address. This innovative approach offers a promising avenue for the rational design of next-generation thermal management materials.

THEORETICAL FRAMEWORK

DFT calculation settings

In our study, we employed first-principles computations using the Vienna *Ab Initio* Simulation Package (VASP),⁵⁹ a powerful tool based on DFT.⁶⁰ This allowed us to accurately model the complex dynamics between ions and electrons, which are essential to our system. We achieved this using the Projector Augmented Wave (PAW)⁶¹ method, in conjunction with an advanced plane wave basis set.

To faithfully depict the intricacies of the exchange-correlation energy terms, we integrated the Perdew–Burke–Ernzerhof (PBE) function^{62,63} within the framework of the Generalized Gradient

15 February 2025 11:32:22

Approximation (GGA).^{64,65} In order to correctly identify the van der Waals interaction, the vdW-DFT-cx method (optB86-vdW)⁶⁶ was used in the calculation. The Brillouin zone was sampled using a Γ -centered grid with a linear KSPACING spacing of approximately 0.25 \AA^{-1} and Gaussian smearing with a width of 0.01 eV . For force calculations, a finer support grid was utilized to enhance numerical accuracy. All calculations were performed with a plane-wave energy cutoff of 520 eV . All parameters were established following the previous study.⁵

Construction of the dataset

The foundation of our investigation lies in the construction of a comprehensive and diverse dataset comprising 1253 structures for graphene/h-BN systems (see details in Table S1 in the [supplementary material](#)). Delving into the intricacies of stacking arrangements and linking modes, our dataset explored a plethora of possibilities for graphene, h-BN, and their heterostructures. Recognizing the impact of larger unit cells in capturing nuanced structural nuances, we systematically considered the influence of external factors such as strain, defects, and perturbations. The resultant training set, hosting a staggering 165704 atoms, stands as a testament to our commitment to comprehensively explore the rich landscape of structural configurations.

MLP configuration

We are dedicated to developing an accurate graphene/h-BN potential with the aid of utilizing the fourth-generation NEP from the GPUMD software package.^{54,67} It entailed the strategic use of a multi-layer perceptron architecture with a meticulously designed single hidden layer. The intricacies of the atomic environment descriptor were brought to life by a judicious combination of

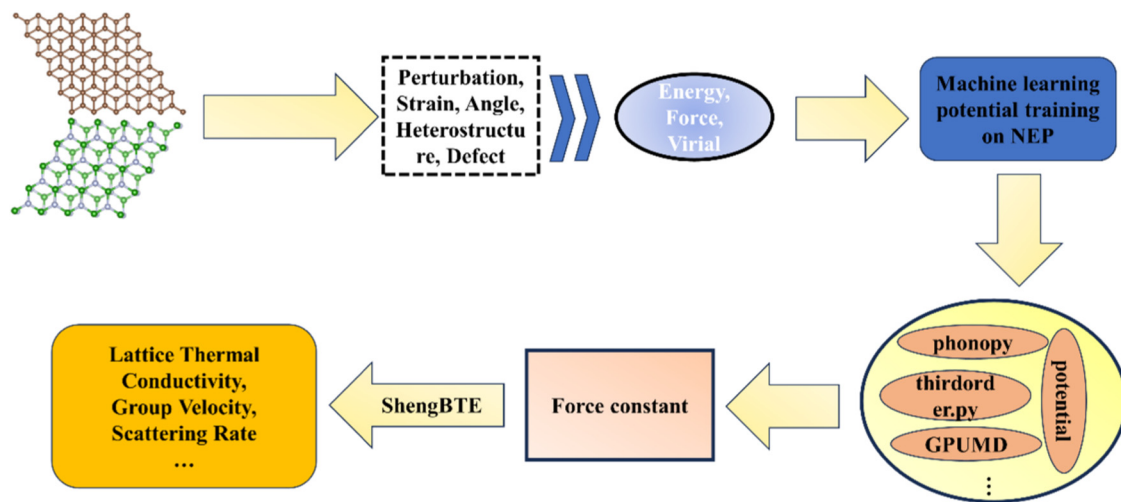
Chebyshev basis functions for the radial part and Legendre polynomials for the three-body angle part. A carefully chosen cutoff of 8 \AA for the radial component and 3.5 \AA for the angular component ensured the fidelity of our MLP architecture, which consistently featured 50 neurons in the hidden layer throughout the entire training process.

Other relevant computational parameters

Our pursuit of a comprehensive understanding extended beyond the confines of the theoretical framework, integrating machine learning potentials with various computational tools. Collaborating seamlessly with GPUMD, phonopy, and shengBTE,^{54,68,69} we embarked on an exploration to extract phononic properties and correlate them with the intricate thermal behaviors of our system.

RESULTS AND DISCUSSION

The process of constructing a complete MLP and predicting the thermal transport properties through MLP is shown in [Fig. 1](#). We search for training structures to obtain energy, force, and virial information for machine learning to acquire MLP, and get the corresponding force constants through the interface with different software and MLP. We then obtain thermal transport-related information using shengBTE, a software that solves the phonon Boltzmann transport equation. In the construction of the training set, we start with pristine multilayer graphene and h-BN as the initial structures, simulating 5000 steps with an AIMD time step of 2 fs, taking one configuration every 100 steps for a constant pressure annealing simulation at 300–1500 K. After obtaining the initial configurations, we apply perturbations, strains, and defects to the initial configurations and perform static calculations to obtain the corresponding energy, force, and virial information to better fit an



15 February 2025 11:32:22

FIG. 1. The methodology for deriving a machine learning potential and evaluating its performance is depicted. The process begins by exposing initial structures to perturbations, strains, angles, heterostructure configurations, and defects to create a comprehensive dataset that includes energy, force, and virial information. This collected data serves as the basis for training a precise machine learning potential function within the NEP framework. Once developed, the potential function is utilized to simulate and predict thermal transport properties through the integration with specialized software interfaces.

appropriate potential energy surface. The 2–4 structures were randomly chosen from the displacement POSCAR files generated using phonopy. These selected configurations served as the perturbed configurations, augmenting the diversity within our dataset and strengthening the robustness of our analysis. Moreover, larger supercells have more positional and angular information, providing more operational space for building an MLP suitable for twisted systems. Larger supercells offer more operational space for constructing MLP for distorted systems like twisted graphene, accommodating varied atomic arrangements and capturing intricate structural features during training. This enhancement in structural detail is crucial for accurately modeling bonding and interaction phenomena in distorted systems, enriching the robustness and fidelity of the study.^{70,71} Essentially, twisted systems are caused by the deviation of the original atomic positions and angles, which changes the potential energy surface. If all possible positions and angles can be expressed, information on different twist angles will also be included. Previous research found that a larger rotating crystal cell system contains rich positional and angular information. Therefore, we constructed twisted structures of graphene and h-BN, with no fewer than 100 atoms in each possible twisted structure. We further choose structures with twist angles of 21.78°, 27.8°, 13.17°, and 9.43° from among these structures for AIMD annealing simulations at 300–1500 K to observe the evolution of twist angles at different temperatures. In our AIMD simulations, conducted over the temperature range of 300 to 1500 K, we replicated an annealing process to emulate real-world conditions. Throughout these simulations, we saved configurations every 100 fs, allowing for a comprehensive sampling of thermal fluctuations. This meticulous approach ensures the robustness of our training dataset.

Notably, our trained MLP meticulously encompasses essential features of multilayer systems, including a range of stackings, interlayer distances, and structural arrangements. By leveraging DFT data calculated with VASP as the foundation of our training set, we introduce an intrinsic periodicity, reinforcing the MLP's capacity to accurately articulate the properties of multilayer systems^{72,73} (for further details, refer to Fig. S2 in the [supplementary material](#)).

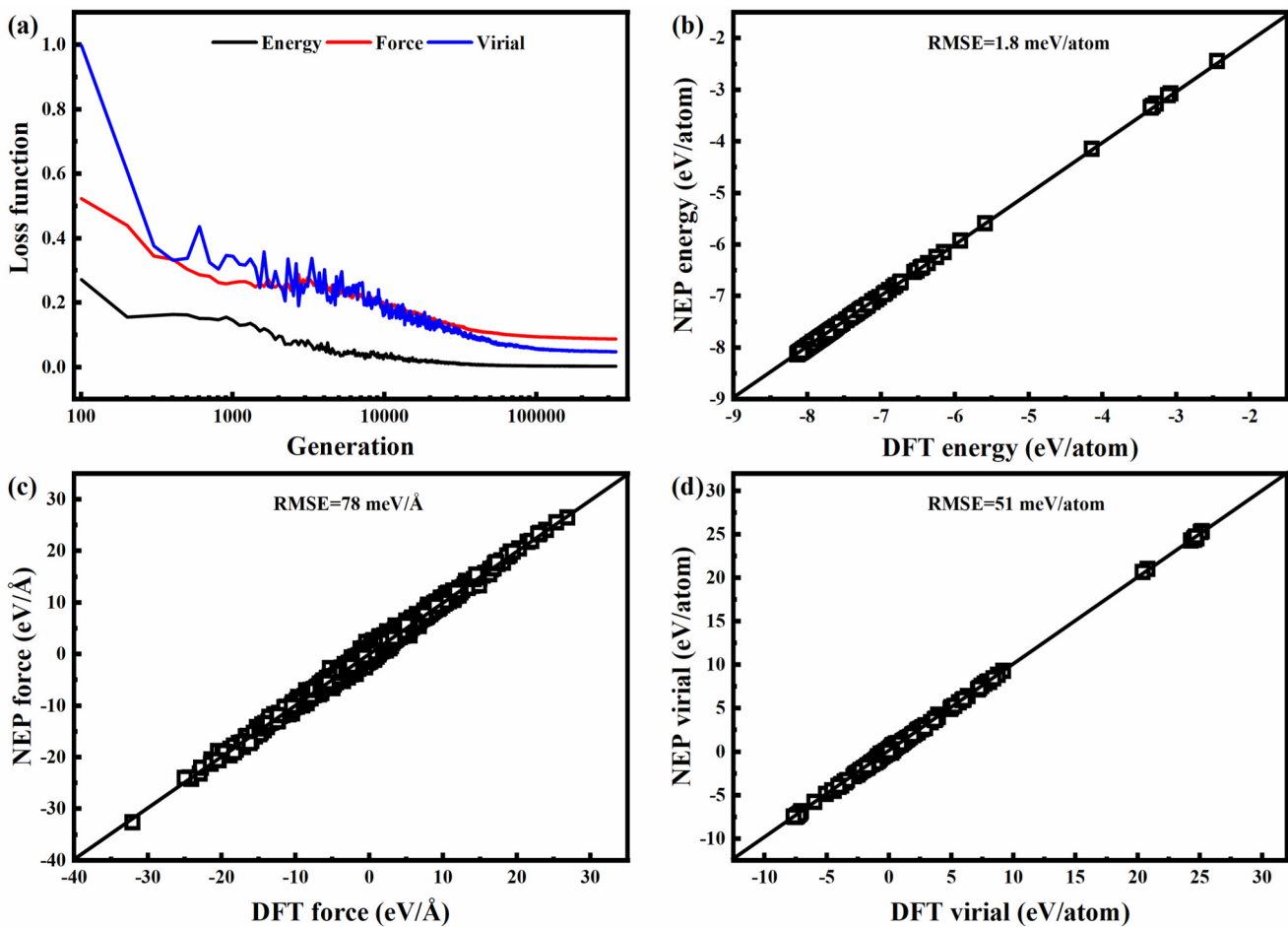
Constructing a unified potential for graphene, h-BN, and their heterostructures is very challenging. On the one hand, it needs to consider all possible situations of graphene and h-BN alone, which has been solved in the initial construction of the training set; on the other hand, the problem of lattice mismatch in heterostructures becomes the key to restricting the unified potential. However, graphene and h-BN have very similar lattice constants, making their layered heterostructures naturally have low lattice mismatch, which solves the second problem smoothly. Therefore, we constructed two initial structures of graphene/h-BN lateral heterostructures and vdW heterostructures and considered twist angles in vdW heterostructures as in single graphene and h-BN to fully consider possible atomic positions and angles. Finally, we constructed a training set containing 1253 structures with 165704 atoms, fully obtaining energy, force, and virial information to realize the scanning of potential energy surfaces in machine learning processes and performing MLP of graphene, h-BN, and their heterostructures under a unified descriptor.

Through the fourth-generation NEP framework built into GPUMLD, we fit the training set with MLP to obtain a unified MLP. In this process, we set the training steps to 350 000 steps to obtain a convergent MLP. As shown in [Fig. 2\(a\)](#), when the training steps reach 200 000 steps, the loss functions of energy, force, and virial have fully converged, indicating that a fully convergent MLP has been obtained. A further comparison of the trained energy, force, and virial with DFT results is shown in [Figs. 2\(b\)–2\(d\)](#). The root mean square errors (RMSEs) for energy, force, and virial are 1.8 meV/atom, 78 meV/Å, and 51 meV/atom, respectively. Comparatively, previously reported RMSE values for h-BN are 2 meV/atom, 45 meV/Å, and 13 meV/atom, while for graphene, they are 1 meV/atom, 43 meV/Å, and 8 meV/atom.^{5, 55} These results indicate that the trained MLP exhibits high consistency with DFT and achieves DFT-level accuracy.

While maintaining a high consistency in energy, force, and virial with DFT during training tests is important, it does not guarantee similar consistency during the application process, especially in the study of thermal transport. In this context, an accurate prediction of lattice constants and dispersion relationships becomes essential. It is widely acknowledged that the precision of lattice constants and dispersion relationships significantly influences the ability to predict lattice thermal conductivity within a reasonable order of magnitude. Therefore, we verified the lattice constants of graphite, graphene, AB stacked graphene, bulk h-BN, monolayer h-BN, and AB stacked h-BN compared with experiments or DFT calculations. As shown in [Table I](#), where “a” and “c” represent the lattice directions, CBN-NEP shows good predictive performance in all verified systems. This suggests that CBN-NEP can correctly identify lattice constants.

In the phonon gas model, the depiction of lattice vibration relies on the spacing between atoms. CBN-NEP's precise prediction of lattice constants establishes a strong basis for accurately forecasting lattice vibration. The accuracy of identifying lattice vibration can be assessed through the phonon dispersion relationship, by comparing the results of DFT and CBN-NEP calculations for AB stacked graphene and h-BN, as depicted in [Figs. 3\(a\) and 3\(b\)](#). It becomes evident that CBN-NEP excels in capturing information related to lattice vibrations, particularly in the phonon dispersion relationship. Unlike traditional empirical potential fields that lack accuracy in describing high-frequency phonons, CBN-NEP demonstrates excellent performance in characterizing high-frequency lattice vibration.

In addition to harmonic lattice vibration information in phonon transport, anharmonic interactions among phonons are also crucial. The primary approach for applying DFT to phonon transport research involves obtaining the harmonic and anharmonic interaction force constants between atoms, known as the second-order (IFC2) and third-order (IFC3) force constants. We use the second-order and third-order force constants as input parameters to solve the phonon Boltzmann transport equation, extracting phonon transport-related information. This involves integrating CBN-NEP with phonopy and thriorder.py to compute the force constants of AB stacked graphene. Then, using the shengBTE software package, we derive the corresponding thermal conductivity. In [Fig. 3\(c\)](#), we show the thermal conductivity acquired using both DFT and CBN-NEP from 300 K to 1500 K. A



15 February 2025 11:32:22

FIG. 2. Training model results. (a) Represents the convergence of energy, force, and virial loss functions during training. (b), (c), and (d) illustrate the comparison error results of energy, force, and virial predicted by using NEP and DFT throughout the training process, with RMSE representing the root mean square error.

comparison of thermal conductivity demonstrates the consistency of CBN-NEP with DFT across a broad temperature spectrum. The thermal conductivity at room temperature for AB stacked graphene and h-BN is 1893 and 246 W/m-K, respectively, aligning with

TABLE I. Comparison of lattice constants. The lattice constants are predicted by using NEP, and the inside brackets are determined by using DFT or experiments. (a) and (c) represent the lattice constants in the in-plane and out-of-plane directions, respectively.

Name	Lattice constant (Å)	
	a	c
Graphite	2.465 (2.45) ⁷⁴	6.726 (6.74) ⁷⁴
Graphene	2.465 (2.457) ⁷⁵	
Bilayer graphene	2.466 (2.46) ⁷⁶	
h-BN	2.514 (2.52) ⁷⁷	6.529 (6.67) ⁷⁷
Monolayer h-BN	2.519 (2.51) ⁷⁸	
Bilayer h-BN	2.516 (2.512) ⁷⁸	

those of previous research findings.^{10,79–84} Additionally, the Grüneisen parameter serves as an indicator of the strength of anharmonic interactions in nonharmonic interactions, making it a pivotal parameter for nonharmonic assessment. Therefore, we compare the total Grüneisen parameter between DFT and CBN-NEP results, as illustrated in Fig. 3(c). Across the temperature range of 300 to 1500 K, both DFT and CBN-NEP obtained total Grüneisen parameters exhibit consistent trends. This indicates that CBN-NEP effectively discerns harmonic and nonharmonic vibration information.

Up to now, we have demonstrated the consistency of CBN-NEP with DFT in bilayer graphene and h-BN concerning phonon dispersion relations, lattice thermal conductivity, and anharmonicity. Next, we extended the application of CBN-NEP to explore the thermal behavior of double-layer twisted graphene, h-BN, and graphene/h-BN heterostructures, affirming its suitability for twisted systems. In these systems, the interlayer twist angle disrupts the original symmetry of the structure, leading to a dramatic increase in the number of atoms within the unit cell under twisting.

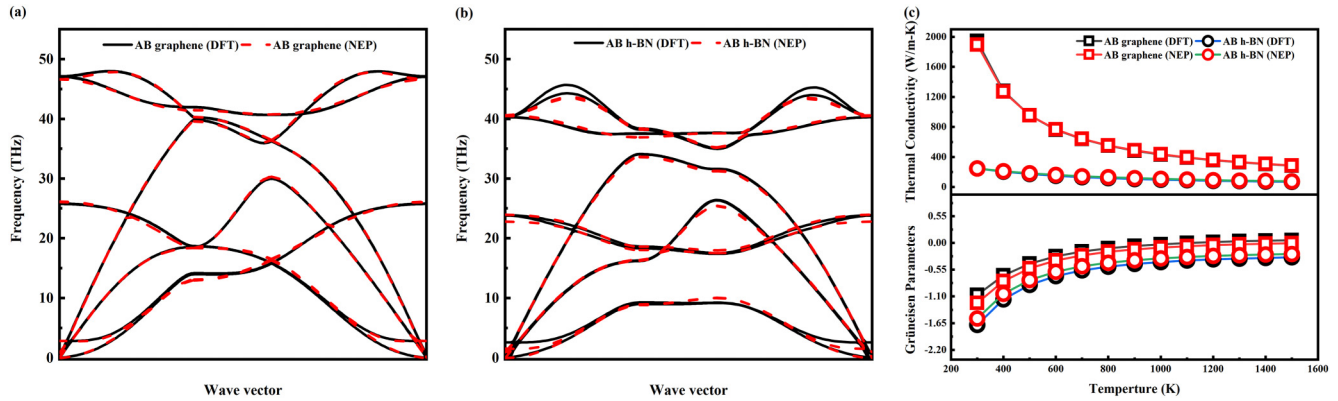


FIG. 3. Phonon dispersion, thermal conductivity, and Grüneisen parameter. (a) and (b) depict the phonon dispersion of AB stacking graphene and h-BN, respectively, with the solid black lines representing DFT results and dotted red lines representing NEP predictions. (c) illustrates the comparison of lattice thermal conductivity and the total Grüneisen parameter of AB stacked graphene and h-BN.

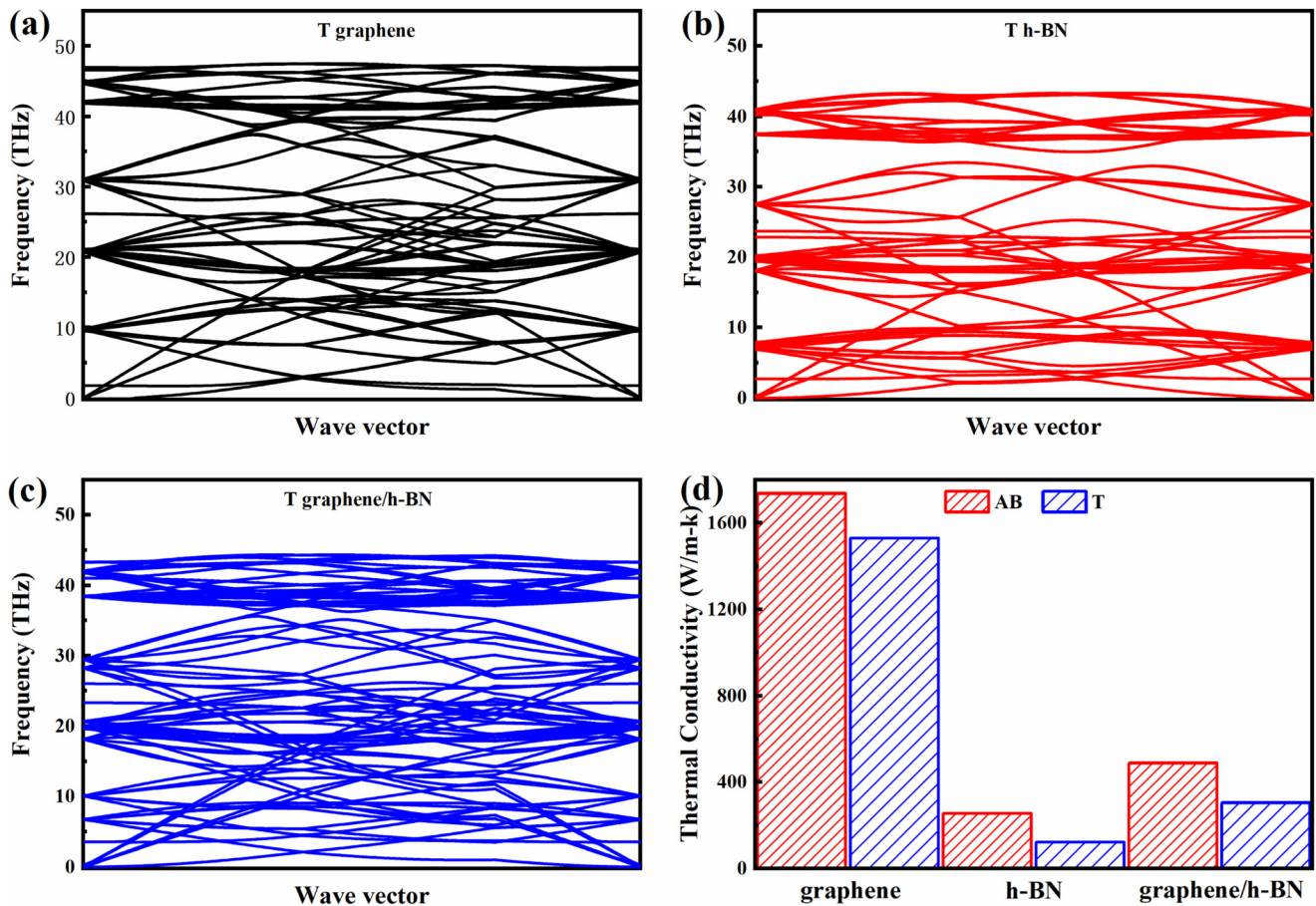
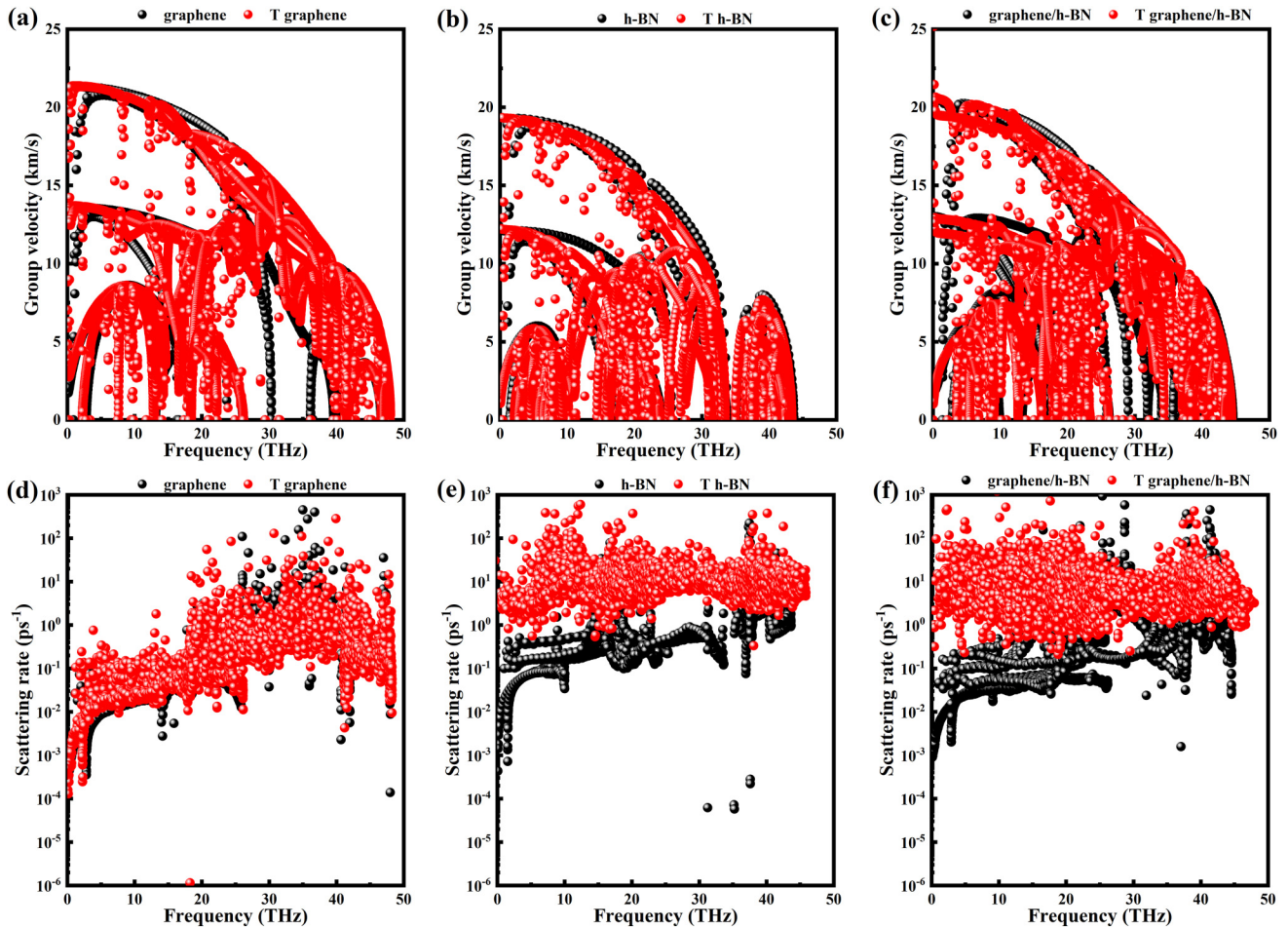


FIG. 4. Phonon dispersion and thermal conductivity. (a) to (c) illustrate the phonon dispersion relationships of graphene, h-BN, and graphene/h-BN heterostructures at an angle of 21.78°, respectively. (d) presents the thermal conductivity of graphene, h-BN, and graphene/h-BN at 300 K, where red indicates the AB stack, and blue indicates the 21.78° rotation.

15 February 2025 11:32:22



15 February 2025 11:32:22

FIG. 5. Phonon group velocity and scattering rate. (a) to (c) illustrate the group velocities of AB stacked graphene, h-BN, and graphene/h-BN heterostructures, respectively, while (d) to (f) represent the corresponding phonon scattering rate.

For instance, previous research on twisted graphene has indicated that a twist angle of 21.78° results in the smallest unit cell beyond the AA and AB stacking configurations.^{45,46} Limited by the memory requirements of solving the Boltzmann transport equation, we focus solely on the 21.78° twist structure for research, with all subsequent twist angles referring specifically to 21.78° unless otherwise stated.

Through the integration of CBN-NEP and shengBTE software packages, we examined the thermal transport properties of graphene, h-BN, and graphene/hexagonal boron nitride heterostructures at a specific twist angle. As depicted in Figs. 4(a)–4(c), the absence of imaginary frequencies for these materials under twisted configurations signifies their structural stability at the given angle. Notably, within the twisted systems, there is a noticeable softening of low-frequency phonons, with the out-of-plane acoustic (ZA) mode near the gamma point exhibiting an almost flatband profile.

This phenomenon leads to intensified phonon scattering and coupling, corroborating findings from earlier research endeavors.

The previous overlap of optical phonons and acoustic phonons influences the behavior of phonon scattering, which is governed by the conservation of energy and momentum, thus impacting the material's thermal conductivity. As illustrated in Fig. 4(d), the calculated thermal conductivity values for T graphene and T h-BN at 300 K are 1530 and 123 W/m-K, respectively. Furthermore, the thermal conductivity of T graphene/h-BN heterostructures is computed at 305.04 W/m-K. In comparison with the AB-stacked heterostructure's thermal conductivity, the thermal conductivity of the twisted graphene/boron nitride heterostructures has plummeted by over 35%, amounting to merely one-fifth of the twisted graphene's value, yet still significantly surpassing that of the twisted h-BN. The phonon dispersion, thermal conductivity, and Grüneisen parameter of the AB stacked graphene/h-BN

heterostructure, calculated by using both DFT and NEP, are illustrated in Fig. S1 in the [supplementary material](#). The results from both approaches demonstrate consistency, underscoring the accuracy of the CBN-NEP potential. Furthermore, both graphene and h-BN exhibit a decline in their twisted thermal conductivities compared with their AB-stacked counterparts, aligning with previous observations on the diminishing effect of twisting on thermal conductivity.

Delving deeper into the underlying physical principles, we have analyzed the critical equation determining thermal conductivity: $k = \frac{1}{3} \Sigma C_V v^2 \tau$, where C_V denotes the phonon specific heat capacity, v represents the phonon group velocity, and τ stands for the phonon lifetime, inversely related to the phonon scattering rate. [Figures 5\(a\)–5\(c\)](#) illuminate the variations in phonon group velocity, indicating a substantial reduction due to twist-induced phonon mode softening and increased optical phonon–acoustic phonon overlap, which are particularly evident in the twisted heterostructures. Such deceleration often stems from altered interlayer interactions that significantly affect phonon–phonon interaction dynamics.

Additionally, we investigate the consequences of alterations in phonon scattering rates. As shown in [Figs. 5\(d\)–5\(e\)](#), transitioning from an AB-stacked to a twisted structure results in a marked elevation in the phonon scattering rate, indicating that twisting exacerbates anharmonic effects through modified interlayer interactions. The visible change in phonon scattering rates manifests this effect: enhanced anharmonicity leads to increased phonon scattering likelihood and curtailed phonon lifetimes. Within this context, the changes in the graphene system are relatively subtle in comparison with those in the h-BN and heterostructure systems, explaining the comparatively minor impact of twisting on graphene's thermal conductivity. Conversely, the heterostructure system undergoes an order-of-magnitude shift in its scattering rate, precipitating a drastic diminution in phonon lifetimes and consequently impeding phonon transmission. Thus, the concurrent reduction in phonon group velocity and scattering rate culminates in a significant decrease in thermal conductivity under twisted conditions as opposed to the AB-stacked configuration. Despite the twist-induced increase in phonon mode overlap, homostructures do not exhibit the same extent of reduction in phonon group velocity and scattering rate as observed in heterostructures. These divergent outcomes ultimately lead to a more substantial reduction in thermal conductivity for heterostructures relative to homostructures when subjected to identical twist conditions.

SUMMARY

We constructed a training set containing 1253 structures and 165704 atoms, which adequately captures energy, forces, and virial information. Through potential energy surface scanning in the machine learning process, we built a unified MLP for graphene, h-BN, and their heterostructures under a consistent descriptor, which we named CBN-NEP. The trained MLP shows high consistency with DFT and achieve DFT precision. Furthermore, we used CBN-NEP to investigate the thermal properties of bilayer twisted graphene, h-BN, and graphene/h-BN heterostructures to verify their applicability in twisted systems. The results indicate that the

thermal conductivity of twisted graphene/boron nitride heterostructures drops by more than 35%, only one-fourth of that of twisted graphene, but still significantly exceeds the thermal conductivity of twisted h-BN. We conclude that the developed CBN-NEP is a promising tool for studying heat transport in materials with strong phonon anharmonicity or spatial disorder, which are often not accurately treated by traditional empirical potentials or perturbative methods. The MLP offers unparalleled accuracy and adaptability in detecting interlayer heat transfer phenomena in van der Waals materials, providing an innovative analytical tool for delving into the complexities of two-dimensional materials and their structures.

SUPPLEMENTARY MATERIAL

See the supplementary material for a comprehensive overview of the calculation details pertaining to the thermal conductivity, including the phonon dispersion of the three layers of graphene and h-BN, using both DFT and NEP methods. Additionally, the mapping of different elements to corresponding atomic numbers and structural counts is also contained.

ACKNOWLEDGMENTS

This research was funded in part by the National Natural Science Foundation of China (Grant No. 12105242) and by the Yunnan Fundamental Research Project (Grant Nos. 202201AT070161, 202301AW070006, and 202401AT07031).

AUTHOR DECLARATIONS

Conflict of interest

The authors have no conflicts to disclose.

Author Contributions

R.C. and Y.T. contributed equally to this work.

Rongkun Chen: Conceptualization (equal); Data curation (equal); Investigation (equal); Writing – original draft (equal). **Yu Tian:** Formal analysis (equal); Methodology (equal); Validation (equal); Writing – original draft (equal). **Jiayi Cao:** Investigation (equal); Software (equal). **Weina Ren:** Conceptualization (equal); Investigation (equal); Software (equal); Validation (equal); Visualization (equal); Writing – review & editing (equal). **Shiqian Hu:** Conceptualization (lead); Funding acquisition (lead); Supervision (lead); Validation (lead); Writing – original draft (lead); Writing – review & editing (lead). **Chunhua Zeng:** Conceptualization (equal); Supervision (equal); Writing – review & editing (equal).

DATA AVAILABILITY

The data that support the findings of this study are available from the corresponding author upon reasonable request.

REFERENCES

- ¹R. McKinney, P. Gorai, E. S. Toberer, and V. Stevanović, "Rapid prediction of anisotropic lattice thermal conductivity: Application to layered materials," *Chem. Mater.* **31**(6), 2048–2057 (2019).
- ²S. E. Kim, F. Mujid, A. Rai, F. Eriksson, J. Suh, P. Poddar, A. Ray, C. Park, E. Fransson, Y. Zhong, D. A. Muller, P. Erhart, D. G. Cahill, and J. Park, "Extremely anisotropic van der Waals thermal conductors," *Nature* **597**(7878), 660–665 (2021).
- ³J. S. Kang, M. Ke, and Y. Hu, "Ionic intercalation in two-dimensional van der Waals materials: *In situ* characterization and electrochemical control of the anisotropic thermal conductivity of black phosphorus," *Nano Lett.* **17**(3), 1431–1438 (2017).
- ⁴Y. Wang, N. Xu, D. Li, and J. Zhu, "Thermal properties of two dimensional layered materials," *Adv. Funct. Mater.* **27**(19), 1604134 (2017).
- ⁵F. Eriksson, E. Fransson, C. Linderålv, Z. Fan, and P. Erhart, "Tuning the through-plane lattice thermal conductivity in van der Waals structures through rotational (dis)ordering," *ACS Nano* **17**(24), 25565–25574 (2023).
- ⁶L. F. C. Pereira, B. Mortazavi, M. Makaremi, and T. Rabczuk, "Anisotropic thermal conductivity and mechanical properties of phagraphene: A molecular dynamics study," *RSC Adv.* **6**(63), 57773–57779 (2016).
- ⁷Z. Fan, L. F. C. Pereira, P. Hirvonen, M. M. Ervasti, K. R. Elder, D. Donadio, T. Ala-Nissila, and A. Harju, "Thermal conductivity decomposition in two-dimensional materials: Application to graphene," *Phys. Rev. B* **95**(14), 144309 (2017).
- ⁸E. Pop, V. Varshney, and A. K. Roy, "Thermal properties of graphene: Fundamentals and applications," *MRS Bull.* **37**(12), 1273–1281 (2012).
- ⁹P. Jiang, X. Qian, R. Yang, and L. Lindsay, "Anisotropic thermal transport in bulk hexagonal boron nitride," *Phys. Rev. Mater.* **2**(6), 064005 (2018).
- ¹⁰S. Matei, K. Yang, X. Liu, S. Huang, J. Wang, L. H. Li, P. Hodgson, M. Zhou, J. He, and Y. Chen, "Bulk hexagonal boron nitride with a quasi-isotropic thermal conductivity," *Adv. Funct. Mater.* **28**(28), 1707556 (2018).
- ¹¹S. Zhao, R. Kitaura, P. Moon, M. Koshino, and F. Wang, "Interlayer interactions in 1D van der Waals moiré superlattices," *Adv. Sci.* **9**(2), 2103460 (2022).
- ¹²Y. Xiao, J. Liu, and L. Fu, "Moiré is more: Access to New properties of two-dimensional layered materials," *Matter* **3**(4), 1142–1161 (2020).
- ¹³D. Halbertal, S. Shabani, A. N. Passupathy, and D. N. Basov, "Extracting the strain matrix and twist angle from the moiré superlattice in van der Waals heterostructures," *ACS Nano* **16**(1), 1471–1476 (2022).
- ¹⁴M. H. Naik, E. C. Regan, Z. Zhang, Y.-H. Chan, Z. Li, D. Wang, Y. Yoon, C. S. Ong, W. Zhao, S. Zhao, M. I. B. Utama, B. Gao, X. Wei, M. Sayyad, K. Yumigeta, K. Watanabe, T. Taniguchi, S. Tongay, F. H. Da Jornada, F. Wang, and S. G. Louie, "Intralayer charge-transfer moiré excitons in van der Waals superlattices," *Nature* **609**(7925), 52–57 (2022).
- ¹⁵W. Ren, S. Lu, C. Yu, J. He, Z. Zhang, J. Chen, and G. Zhang, "Impact of moiré superlattice on atomic stress and thermal transport in van der Waals heterostructures," *Appl. Phys. Rev.* **10**(4), 041404 (2023).
- ¹⁶G. Chen, A. L. Sharpe, P. Gallagher, I. T. Rosen, E. J. Fox, L. Jiang, B. Lyu, H. Li, K. Watanabe, T. Taniguchi, J. Jung, Z. Shi, D. Goldhaber-Gordon, Y. Zhang, and F. Wang, "Signatures of tunable superconductivity in a trilayer graphene moiré superlattice," *Nature* **572**(7768), 215–219 (2019).
- ¹⁷J. Song and M. Sun, "Modulating thermoelectric properties of the MoSe₂/WSe₂ superlattice heterostructure by twist angles," *ACS Appl. Mater. Interfaces* **16**(3), 3325–3333 (2024).
- ¹⁸M.-L. Lin, Q.-H. Tan, J.-B. Wu, X.-S. Chen, J.-H. Wang, Y.-H. Pan, X. Zhang, X. Cong, J. Zhang, W. Ji, P.-A. Hu, K.-H. Liu, and P.-H. Tan, "Moiré phonons in twisted bilayer MoS₂," *ACS Nano* **12**(8), 8770–8780 (2018).
- ¹⁹Z. Li, J.-M. Lai, and J. Zhang, "Review of phonons in moiré superlattices," *J. Semicond.* **44**(1), 011902 (2023).
- ²⁰Z. Zhang, S. Hu, J. Chen, and B. Li, "Hexagonal boron nitride: A promising substrate for graphene with high heat dissipation," *Nanotechnology* **28**(22), 225704 (2017).
- ²¹Y. Li, F. Zhang, V.-A. Ha, Y.-C. Lin, C. Dong, Q. Gao, Z. Liu, X. Liu, S. H. Ryu, H. Kim, C. Jozwiak, A. Bostwick, K. Watanabe, T. Taniguchi, B. Kousa, X. Li, E. Rotenberg, E. Khalaf, J. A. Robinson, F. Giustino, and C.-K. Shih, "Tuning commensurability in twisted van der Waals bilayers," *Nature* **625**(7995), 494–499 (2024).
- ²²C. Yuan, J. Li, L. Lindsay, D. Cherns, J. W. Pomeroy, S. Liu, J. H. Edgar, and M. Kuball, "Modulating the thermal conductivity in hexagonal boron nitride via controlled boron isotope concentration," *Commun. Phys.* **2**(1), 43 (2019).
- ²³I. Brihuega, P. Mallet, H. González-Herrero, G. Trambly De Laissardiére, M. M. Ugeda, L. Magaud, J. M. Gómez-Rodríguez, F. Ynduráin, and J.-Y. Veuillen, "Unraveling the intrinsic and robust nature of van hove singularities in twisted bilayer graphene by scanning tunneling microscopy and theoretical analysis," *Phys. Rev. Lett.* **109**(19), 196802 (2012).
- ²⁴S. Duan, Y. Cui, W. Yi, X. Chen, B. Yang, and X. Liu, "Enhanced thermoelectric performance in black phosphorene via tunable interlayer twist," *Small* **18**(49), 2204197 (2022).
- ²⁵N. Kumar, A. Chaudhuri, V. Arya, C. Bakli, and C. Bera, "Significantly reduced thermal conductivity and enhanced thermoelectric performance of twisted bilayer graphene," *J. Appl. Phys.* **134**(4), 044301 (2023).
- ²⁶S. Mandal, I. Maity, A. Das, M. Jain, and P. K. Maiti, "Tunable lattice thermal conductivity of twisted bilayer MoS₂," *Phys. Chem. Chem. Phys.* **24**(22), 13860–13868 (2022).
- ²⁷K. Kim, J. He, B. Ganeshan, and J. Liu, "Disorder enhanced thermal conductivity anisotropy in two-dimensional materials and van der Waals heterostructures," *J. Appl. Phys.* **124**(5), 055104 (2018).
- ²⁸D. Rhodes, S. H. Chae, R. Ribeiro-Palau, and J. Hone, "Disorder in van der Waals heterostructures of 2D materials," *Nat. Mater.* **18**(6), 541–549 (2019).
- ²⁹Y. Liu, N. O. Weiss, X. Duan, H.-C. Cheng, Y. Huang, and X. Duan, "van der Waals heterostructures and devices," *Nat. Rev. Mater.* **1**(9), 16042 (2016).
- ³⁰A. K. Geim and I. V. Grigorieva, "van der Waals heterostructures," *Nature* **499**(7459), 419–425 (2013).
- ³¹C. Jin, E. Y. Ma, O. Karni, E. C. Regan, F. Wang, and T. F. Heinz, "Ultrafast dynamics in van der Waals heterostructures," *Nat. Nanotechnol.* **13**(11), 994–1003 (2018).
- ³²M. Huang, S. Li, Z. Zhang, X. Xiong, X. Li, and Y. Wu, "Multifunctional high-performance van der Waals heterostructures," *Nat. Nanotechnol.* **12**(12), 1148–1154 (2017).
- ³³M. S. Islam, I. Mia, A. S. M. J. Islam, C. Stampfl, and J. Park, "Temperature and interlayer coupling induced thermal transport across graphene/2D-SiC van der Waals heterostructure," *Sci. Rep.* **12**(1), 761 (2022).
- ³⁴Y. Yang, J. Ma, Q.-X. Pei, J. Yang, and Y. Zhang, "Cross-plane thermal transport in multiplayer graphene/h-BN van der Waals heterostructures: The role of interface morphology," *Int. J. Heat Mass Transf.* **216**, 124558 (2023).
- ³⁵X.-K. Chen, Z.-X. Xie, W.-X. Zhou, L.-M. Tang, and K.-Q. Chen, "Thermal rectification and negative differential thermal resistance behaviors in graphene/hexagonal boron nitride heterojunction," *Carbon* **100**, 492–500 (2016).
- ³⁶T. Ma, P. Chakraborty, X. Guo, L. Cao, and Y. Wang, "First-principles modeling of thermal transport in materials: Achievements, opportunities, and challenges," *Int. J. Thermophys.* **41**(1), 9 (2020).
- ³⁷V. L. Deringer, M. A. Caro, and G. Csányi, "Machine learning interatomic potentials as emerging tools for materials science," *Adv. Mater.* **31**(46), 1902765 (2019).
- ³⁸H.-Y. Ko, J. Jia, B. Santra, X. Wu, R. Car, and R. A. DiStasio, Jr., "Enabling large-scale condensed-phase hybrid density functional theory based *Ab initio* molecular dynamics. 1. Theory, algorithm, and performance," *J. Chem. Theory Comput.* **16**(6), 3757–3785 (2020).
- ³⁹S. Axelrod, D. Schwalbe-Koda, S. Mohapatra, J. Damewood, K. P. Greenman, and R. Gómez-Bombarelli, "Learning matter: Materials design with machine learning and atomistic simulations," *Acc. Mater. Res.* **3**(3), 343–357 (2022).
- ⁴⁰S. Dong, A. Zhang, K. Liu, J. Ji, Y. G. Ye, X. G. Luo, X. H. Chen, X. Ma, Y. Jie, C. Chen, X. Wang, and Q. Zhang, "Ultralow-Frequency collective compression mode and strong interlayer coupling in multilayer black phosphorus," *Phys. Rev. Lett.* **116**(8), 087401 (2016).

- ⁴¹C. Zhang, C.-P. Chuu, X. Ren, M.-Y. Li, L.-J. Li, C. Jin, M.-Y. Chou, and C.-K. Shih, "Interlayer couplings, moiré patterns, and 2D electronic superlattices in MoS₂/WSe₂ hetero-bilayers," *Sci. Adv.* **3**(1), e1601459 (2017).
- ⁴²H. Zheng, B. Wu, S. Li, J. He, K. Chen, Z. Liu, and Y. Liu, "Evidence for inter-layer coupling and moiré excitons in twisted WS₂/WS₂ homostructure superlattices," *Nano Res.* **16**(2), 3429–3434 (2023).
- ⁴³R. Samajdar and M. S. Scheurer, "Microscopic pairing mechanism, order parameter, and disorder sensitivity in moiré superlattices: Applications to twisted double-bilayer graphene," *Phys. Rev. B* **102**(6), 064501 (2020).
- ⁴⁴G. Abbas, Y. Li, H. Wang, W. Zhang, C. Wang, and H. Zhang, "Recent advances in twisted structures of flatland materials and crafting moiré superlattices," *Adv. Funct. Mater.* **30**(36), 2000878 (2020).
- ⁴⁵J. Wang, Y. Zheng, A. J. Millis, and J. Cano, "Chiral approximation to twisted bilayer graphene: Exact intravalley inversion symmetry, nodal structure, and implications for higher magic angles," *Phys. Rev. Res.* **3**(2), 023155 (2021).
- ⁴⁶M. He, Y. Li, J. Cai, Y. Liu, K. Watanabe, T. Taniguchi, X. Xu, and M. Yankowitz, "Symmetry breaking in twisted double bilayer graphene," *Nat. Phys.* **17**(1), 26–30 (2021).
- ⁴⁷J. A. Harrison, J. D. Schall, S. Maskey, P. T. Mikulski, M. T. Knippenberg, and B. H. Morrow, "Review of force fields and intermolecular potentials used in atomistic computational materials research," *Appl. Phys. Rev.* **5**(3), 031104 (2018).
- ⁴⁸K. Wan, J. He, and X. Shi, "Construction of high accuracy machine learning interatomic potential for surface/interface of nanomaterials—A review," *Adv. Mater.* 2305758 (published online) (2023).
- ⁴⁹J. Behler and M. Parrinello, "Generalized neural-network representation of high-dimensional potential-energy surfaces," *Phys. Rev. Lett.* **98**(14), 146401 (2007).
- ⁵⁰A. P. Bartók, M. C. Payne, R. Kondor, and G. Csányi, "Gaussian approximation potentials: The accuracy of quantum mechanics, without the electrons," *Phys. Rev. Lett.* **104**(13), 136403 (2010).
- ⁵¹S. Chmiela, A. Tkatchenko, H. E. Sauceda, I. Poltavsky, K. T. Schütt, and K.-R. Müller, "Machine learning of accurate energy-conserving molecular force fields," *Sci. Adv.* **3**(5), e1603015 (2017).
- ⁵²I. S. Novikov, K. Gubaev, E. V. Podryabinkin, and A. V. Shapeev, "The MLIP package: Moment tensor potentials with MPI and active learning," *Mach. Learn. Sci. Technol.* **2**(2), 025002 (2021).
- ⁵³H. Wang, L. Zhang, J. Han, and W. E, "DeepPMD-kit: A deep learning package for many-body potential energy representation and molecular dynamics," *Comput. Phys. Commun.* **228**, 178–184 (2018).
- ⁵⁴Z. Fan, Z. Zeng, C. Zhang, Y. Wang, K. Song, H. Dong, Y. Chen, and T. Ala-Nissila, "Neuroevolution machine learning potentials: Combining high accuracy and low cost in atomistic simulations and application to heat transport," *Phys. Rev. B* **104**(10), 104309 (2021).
- ⁵⁵P. Rowe, V. L. Deringer, P. Gasparotto, G. Csányi, and A. Michaelides, "An accurate and transferable machine learning potential for carbon," *J. Chem. Phys.* **153**(3), 034702 (2020).
- ⁵⁶B. Wang, P. Ying, and J. Zhang, "The thermoelastic properties of monolayer covalent organic frameworks studied by machine-learning molecular dynamics," *Nanoscale* **16**(1), 237–248 (2024).
- ⁵⁷Q. Li, M. Liu, Y. Zhang, and Z. Liu, "Hexagonal boron nitride-graphene heterostructures: Synthesis and interfacial properties," *Small* **12**(1), 32–50 (2016).
- ⁵⁸R. Li, E. Lee, and T. Luo, "A unified deep neural network potential capable of predicting thermal conductivity of silicon in different phases," *Mater. Today Phys.* **12**, 100181 (2020).
- ⁵⁹J. Hafner, "Ab-initio simulations of materials using VASP: Density-functional theory and beyond," *J. Comput. Chem.* **29**(13), 2044–2078 (2008).
- ⁶⁰D. Bagayoko, "Understanding density functional theory (DFT) and completing it in practice," *AIP Adv.* **4**(12), 127104 (2014).
- ⁶¹P. E. Blöchl, "Projector augmented-wave method," *Phys. Rev. B* **50**(24), 17953–17979 (1994).
- ⁶²H. Peng and J. P. Perdew, "Rehabilitation of the Perdew-Burke-Ernzerhof generalized gradient approximation for layered materials," *Phys. Rev. B* **95**(8), 081105 (2017).
- ⁶³B. Hammer, L. B. Hansen, and J. K. Nørskov, "Improved adsorption energetics within density-functional theory using revised Perdew-Burke-Ernzerhof functionals," *Phys. Rev. B* **59**(11), 7413–7421 (1999).
- ⁶⁴L. He, F. Liu, G. Hautier, M. J. T. Oliveira, M. A. L. Marques, F. D. Vila, J. J. Rehr, G.-M. Rignanese, and A. Zhou, "Accuracy of generalized gradient approximation functionals for density-functional perturbation theory calculations," *Phys. Rev. B* **89**(6), 064305 (2014).
- ⁶⁵A. Dal Corso, A. Pasquarello, A. Baldereschi, and R. Car, "Generalized-gradient approximations to density-functional theory: A comparative study for atoms and solids," *Phys. Rev. B* **53**(3), 1180–1185 (1996).
- ⁶⁶D. Mejía-Rodríguez, A. Albavera-Mata, E. Fonseca, D.-T. Chen, H.-P. Cheng, R. G. Hennig, and S. B. Trickey, "Barriers to predictive high-throughput screening for spin-crossover," *Comput. Mater. Sci.* **206**, 111161 (2022).
- ⁶⁷Z. Fan, Y. Wang, P. Ying, K. Song, J. Wang, Y. Wang, Z. Zeng, K. Xu, E. Lindgren, J. M. Rahm, A. J. Gabourie, J. Liu, H. Dong, J. Wu, Y. Chen, Z. Zhong, J. Sun, P. Erhart, Y. Su, and T. Ala-Nissila, "GPUMD: A package for constructing accurate machine-learned potentials and performing highly efficient atomistic simulations," *J. Chem. Phys.* **157**(11), 114801 (2022).
- ⁶⁸A. Togo, "First-principles phonon calculations with phonopy and Phono3py," *J. Phys. Soc. Jpn.* **92**(1), 012001 (2023).
- ⁶⁹W. Li, J. Carrete, N. A. Katcho, and N. Mingo, "ShengBTE: A solver of the Boltzmann transport equation for phonons," *Comput. Phys. Commun.* **185**(6), 1747–1758 (2014).
- ⁷⁰J. D. Morrow, J. L. A. Gardner, and V. L. Deringer, "How to validate machine-learned interatomic potentials," *J. Chem. Phys.* **158**(12), 121501 (2023).
- ⁷¹J. Behler and G. Csányi, "Machine learning potentials for extended systems: A perspective," *Eur. Phys. J. B* **94**(7), 142 (2021).
- ⁷²P. Friederich, F. Häse, J. Proppe, and A. Aspuru-Guzik, "Machine-learned potentials for next-generation matter simulations," *Nat. Mater.* **20**(6), 750–761 (2021).
- ⁷³Z. Chen, M. L. Berrens, K.-T. Chan, Z. Fan, and D. Donadio, "Thermodynamics of water and Ice from a fast and scalable first-principles neuroevolution potential," *J. Chem. Eng. Data* **69**(1), 128–140 (2024).
- ⁷⁴I. A. Gospodarev, K. V. Kravchenko, E. S. Syrkina, and S. B. Feodos'ev, "Quasi-two-dimensional features in the phonon spectrum of graphite," *Low Temp. Phys.* **35**(7), 589–595 (2009).
- ⁷⁵A. K. Sahoo and M. R. Panigrahi, "A study on strain and density in graphene-induced Bi₂O₃ thin film," *Bull. Mater. Sci.* **44**(3), 232 (2021).
- ⁷⁶D'Souza and Mukherjee, "First-principles study of the electrical and lattice thermal transport in monolayer and bilayer graphene," *Phys. Rev. B* **95**(8), 085435 (2017).
- ⁷⁷H. Henck, D. Pierucci, G. Fugallo, J. Avila, G. Cassabois, Y. J. Dappe, M. G. Silly, C. Chen, B. Gil, M. Gatti, F. Sottile, F. Sirotti, M. C. Asensio, and A. Ouerghi, "Direct observation of the band structure in bulk hexagonal boron nitride," *Phys. Rev. B* **95**(8), 085410 (2017).
- ⁷⁸U. Paliwal, G. Sharma, and K. B. Joshi, "First-principles characterization of the electronic properties of h-BN layers," *Mater. Today Proc.* **50**(3), 301–306 (2022).
- ⁷⁹M. J. Mezzani, W. Song, P. Wang, F. Lu, Z. Hou, A. Anderson, H. Maimaiti, and Y. Sun, "Boron nitride nanomaterials for thermal management applications," *ChemPhysChem* **16**(7), 1339–1346 (2015).
- ⁸⁰L. Lindsay and D. A. Broido, "Enhanced thermal conductivity and isotope effect in single-layer hexagonal boron nitride," *Phys. Rev. B* **84**(15), 155421 (2011).
- ⁸¹A. I. Cocemasov, D. L. Nika, and A. A. Balandin, "Phonons in twisted bilayer graphene," *Phys. Rev. B* **88**(3), 035428 (2013).
- ⁸²S. Illera, M. Pruneda, L. Colombo, and P. Ordejón, "Thermal and transport properties of pristine single-layer hexagonal boron nitride: A first principles investigation," *Phys. Rev. Mater.* **1**(4), 044006 (2017).
- ⁸³S. Han, X. Nie, S. Gu, W. Liu, L. Chen, H. Ying, L. Wang, Z. Cheng, L. Zhao, and S. Chen, "Twist-angle-dependent thermal conduction in single-crystalline bilayer graphene," *Appl. Phys. Lett.* **118**(19), 193104 (2021).
- ⁸⁴H. Li, H. Ying, X. Chen, D. L. Nika, A. I. Cocemasov, W. Cai, A. A. Balandin, and S. Chen, "Thermal conductivity of twisted bilayer graphene," *Nanoscale* **6**(22), 13402–13408 (2014).